06

As-grown dislocation glide motion in bulk single crystals of AlN: transmission electron microscope study

© A.V. Myasoedov,[1] T.S. Argunova,[1] M.Yu. Gutkin,[2,3] E.N. Mokhov,[1] O.P. Kazarova,[1] S.S. Nagalyuk[1]

[1] Ioffe Institute,
194021 St. Petersburg, Russia
[2] Institute for Problems in Mechanical Engineering of the Russian Academy of Sciences,
199178 St. Petersburg, Russia
[3] ITMO University,
197101 St. Petersburg, Russia
e-mail: argunova@mail.ioffe.ru

Received July 28, 2025
Revised December 21, 2025
Accepted December 23, 2025

AlN single crystals grown by sublimation on SiC substrates have a relatively high density of structural defects. With increasing ingot length, the crystallinity improves and higher quality crystals can be obtained. In this paper, we apply transmission electron microscopy to understand the processes of the reduction of defects. The mechanisms responsible for this reduction have been identified to include dislocation reactions, the formation of low-angle boundaries, and basal dislocation slip. A 2.5 mm thick AlN bulk crystal was grown on a 64 mm diameter SiC substrate using an advanced technology in which a liquid silicon film is present on the growing surface.

Keywords: dislocations, AlN bulk single crystal, SiC substrate, transmission electron microscopy.

DOI: 10.61011/TP.2026.04.63267.200-25

Introduction

High-frequency nitride-gallium electronics is characterized by high specific power, which results in undesirable effects of generation and scattering of heat during operation of electronic devices. A local increase of the temperature, low efficiency of instruments due to defects in a crystal structure and other undesirable phenomena are caused by growing an AlN buffer layer on foreign substrates of sapphire or silicon when producing GaN/AlN heterostructures. Silicon carbide (SiC) substrates or thin SiC/Si films produced by coordinated substitution of atoms [1,2] facilitate the growth of the AlN buffer layers with improved properties. But only native substrates made of AlN crystals provide improvement of crystallinity, high thermal conductivity and no interphase thermal resistance at the same time [3].

Bulk crystals are grown by sublimation by transfer of AlN vapor from a source to a SiC seed due to a temperature gradient (Physical Vapor Transport, PVT) (see, for example, a review [4]). One of general problems arising in the growth process is generation of structural defects. In order to improve a structural quality of an AlN−SiC interface, special seeding conditions are created by building up the buffer layer; then, during long growth, crystallinity is improved with an ingot length increasing. In particular, in order to reduce a defect density, a buffer made as an AlN discontinuous layer with air gaps is grown on the interface [5] and vicinal steps [6] or pyramidal islands [7,8] are formed on the SiC surface. Flat SiC substrates [8] are the best suited for producing industrial-size crystals (with the diameter of ≥ 2 inches). The crystals studied herein are grown by applying a flat substrate, whose surface is wetted by a thin liquid-silicon film during AIN growth [9]. For this purpose, a composition of the AlN source is supplemented with a SiC additive. The present study addresses behavior of as-grown dislocations in such crystals.

The wurtzite-structure AlN crystals are characterized by the following dislocation slip systems: prismatic $\{1\bar{1}00\}\langle 11\bar{2}0\rangle$, pyramidal $\{11\bar{2}2\}\langle 11\bar{2}3\rangle$, $\{10\bar{1}1\}\langle\bar{1}2\bar{1}0\rangle$, $\{10\bar{1}2\}\langle\bar{1}2\bar{1}0\rangle$ and basal $(0001)\langle 11\bar{2}0\rangle$ (see, for example, [10,11]). Threading dislocations (TD) fill a volume of a growing crystal as well as under a condition that they do not interact with other defects and propagate from the interface to a free surface. On the contrary, misfit dislocations are localized near the interface [12] and relieve a stress caused by mismatch of parameters of the SiC and AlN lattices. A number is the basal dislocations (BD) is always smaller than that of the threading dislocations in the crystal bulk. In the best commercial crystals, the BD density does not exceed 3% of the total density of dislocation, which is confirmed by data of methods of X-ray topography and selective surface etching [13].

Presently, properties of dislocations penetrating into the bulk of the AlN crystals from the interface are quite well studied. Much less is known about slip of dislocations in a basal plane. In indentation experiments, it is difficult to activate basal slip and it depends on the total density of the structural defects [11]. Interest of the present study lies in detailed consideration of as-grown dislocations that belong to the prismatic and basal slip systems. By clarifying specific features of processes of propagation and interaction

of dislocations of the various slip systems, it is possible to find a method of growing of the AlN single crystals with an almost defectless crystal structure.

1. Samples and experimental procedure

The crystals have been grown by the sublimation-sandwich method (SSM) [14] in our self-made furnaces with a resistive graphite heater. AlN vapor was sourced from a polycrystalline powder annealed at the temperature $\sim 2100\,^{\circ}$C for purifying from oxygen traces. The SSM is characterized by a small gap between the source and the SiC substrate. The substrate was fixed on butt ends of a TaC container so that a gap width was 5–10 mm. Pressure of nitrogen in the container was 0.3 atm. At the main stage, the crystal was growing at the rate $40-80\,\mu$m·h^{-1} at the temperature 1960 °C–2000 °C.

The growth process was unique in that there was a liquid silicon phase wetting the SiC surface. Silicon can be supplied into a growth zone from the substrate or a silicon-containing source. Moreover, by making sure of its positive effect, SiC pieces can be intentionally added into a sublimated AlN powder. With the temperature increasing to 1600 °C–1800 °C, first the buffer layer is formed. Within the temperature range 1900 °C–2000 °C the growth rate increases. The liquid silicon film is on a growing buffer surface without interfering with the growth rate. There are reasons to believe that the film provides high mobility of adatoms and facilitates implementation of a mechanism of layer-by-layer crystal growth. Nevertheless, an increase of the film thickness and/or surface deterioration of the wettability results in formation of droplets that can dissolve the growing crystal until through holes appear therein. On the other hand, the increase of silicon vapor pressure can cause formation of inclusions.

The AlN single crystal of the thickness of 2.5 mm and the diameter of 64 mm, which is studied herein, is shown in Fig. 1. The crystal has been grown on the (0001)Si-face of the SiC–6H substrate; it has a shining growth surface and a well-developed (0001)Al facet.

The structural defects were studied by the TEM method in electronic microscopes Osiris (FEI Technologies Inc., Hillsboro, Oregon) and Philips EM–420 (Philips, Amsterdam, Netherlands). Samples were cut out of the crystal shown in Fig. 1 at a close distance to the interface and then they were thinned to an electron-transparent thickness. It was achieved by two ways: using a focused ion beam technology (FIB) or by mechanical thinning and ion etching with ions Ar^+ at accelerating voltage of 4 kV until the through hole was formed. Lamellas for FIB were formed in a planar or cross-section geometry, when the lamella surface was parallel to the interface or a crystal growth axis, respectively. The second method was used to create a hole on the surface of the planar sample. At the same time, the ion beam had a grazing surface incidence angle: 7–10°. As a result, the area of foil of the thickness 100–500 nm, which is arranged on a hole edge, had the maximum possible value. The sample prepared by this method is shown in Fig. 2.

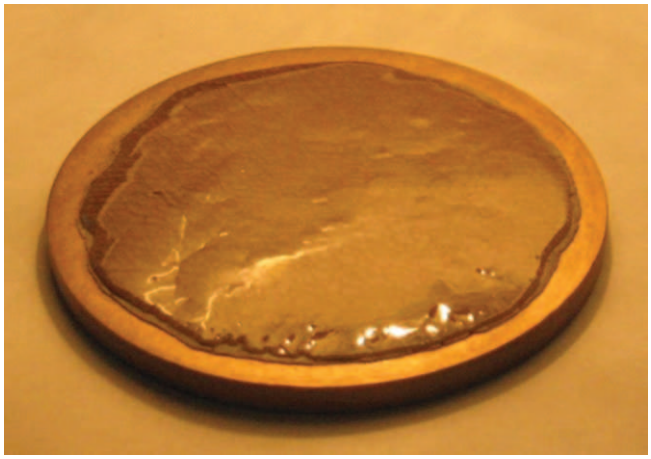

Figure 1. AlN single crystal. The thickness and the diameter of the crystal are 2.5 and 64 mm, respectively. The crystal has been grown on the Si-face of the 6H-SiC substrate by the sublimation sandwich-method, mechanically polished at the substrate side to remove it and glued to a TaC plate. It is shot in reflected light with side illumination.

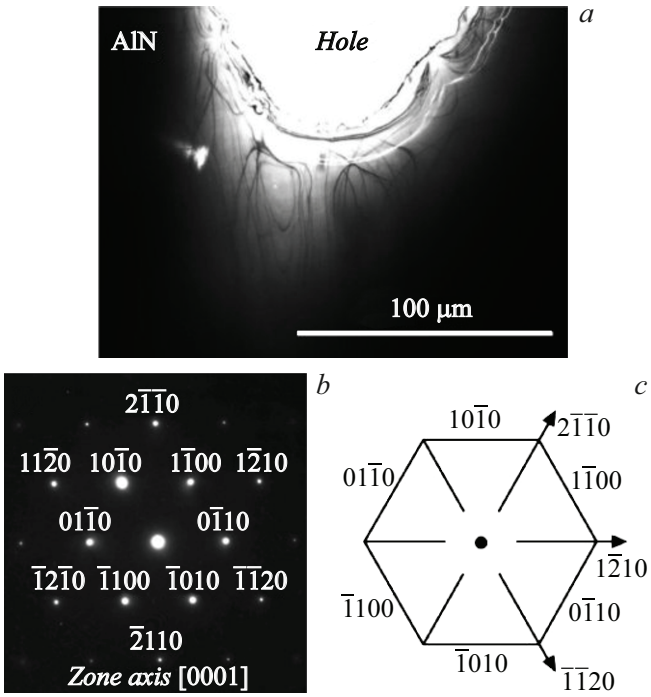

Figure 2. *a* — the sample prepared by chemical-mechanical thinning and etching with the ions Ar^+. The electron-transparent region is arranged on the hole edge; *b* — the electron diffraction pattern of the AlN crystal, which is obtained near the AlN/SiC interface; *c* — the diagram of mutual arrangement and symbols of six lattice planes of AIN (the arrows mark some crystallographic directions).

2. Results and discussion

Fig. 3 demonstrates single TDs and their groups. The TD lines were parallel to the growth axis [0001] or inclined thereto at a certain angle. Fig. 3, *a, b* shows the lamella cut out parallel to the growth direction at the distance $\sim 300\,\mu$m to the AlN/SiC interface. Dislocation visibility variation is related to variation of diffraction conditions described by the diffraction vector **g**. Knowing these conditions, we conclude that the Burgers vector of the dislocation in Fig. 3, *b* is in the direction $[1\bar{2}1\bar{3}]$ (or $[21\bar{1}\bar{3}]$). This TD and other similar TDs belong to the mixed type; their Burgers vectors $\mathbf{b}_{a+c}$ have components along the two axes: a $\langle 11\bar{2}0\rangle$ and c [0001]. In addition to the mixed dislocations, the studied crystal exhibited the TDs of the c- and a-types with the Burgers vectors $\mathbf{b}_c = [0001]$ and $\mathbf{b}_a = (1/3)\langle\bar{1}2\bar{1}0\rangle$, respectively (Fig. 3, *a*).

Fig. 3, *c* is an image of the lamellar cut out parallel to the interface at the distance of $60\,\mu$m. The rosettes of stresses are formed by the TDs distributed with the density $\sim 8 \cdot 10^7$ cm^{-2}. According to an approximate estimate, with an increase of the distance to the interface in 5 times the TD density decreased in 8 times, which does not contradict to a trend of its further reduction to $\sim 10^6$ cm^{-2} at the distance of 1 mm to the interface [5]. Mechanisms of TD density reduction may include annihilation by dislocation reactions, formation of dislocation walls or boundaries and interactions of dislocations with such boundaries. Fig. 3, *d* shows a part of the TDs, which is included in the dislocation walls. By considering them to be tilt boundaries that consist of one row of edge dislocations, it is possible to approximately estimate an angle of rotation around the axis [0001], using only one parameter in doing so — the distance between the dislocations [15]: $D = b/\theta$. Here b is a module of the Burgers vector, θ is a rotation angle and $D \gg b$.

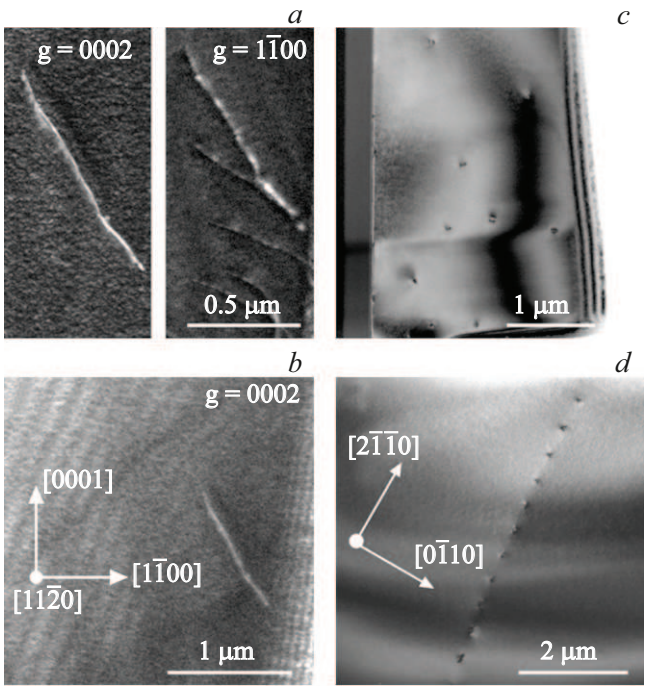

Figure 3. Dark-field images of inclined TDs of the a-type (a) and the mixed type (b). Rosettes of TD stresses, which are identified in the planar sample at the distance of $60\,\mu$m to the interface (c). Dislocation walls (d).

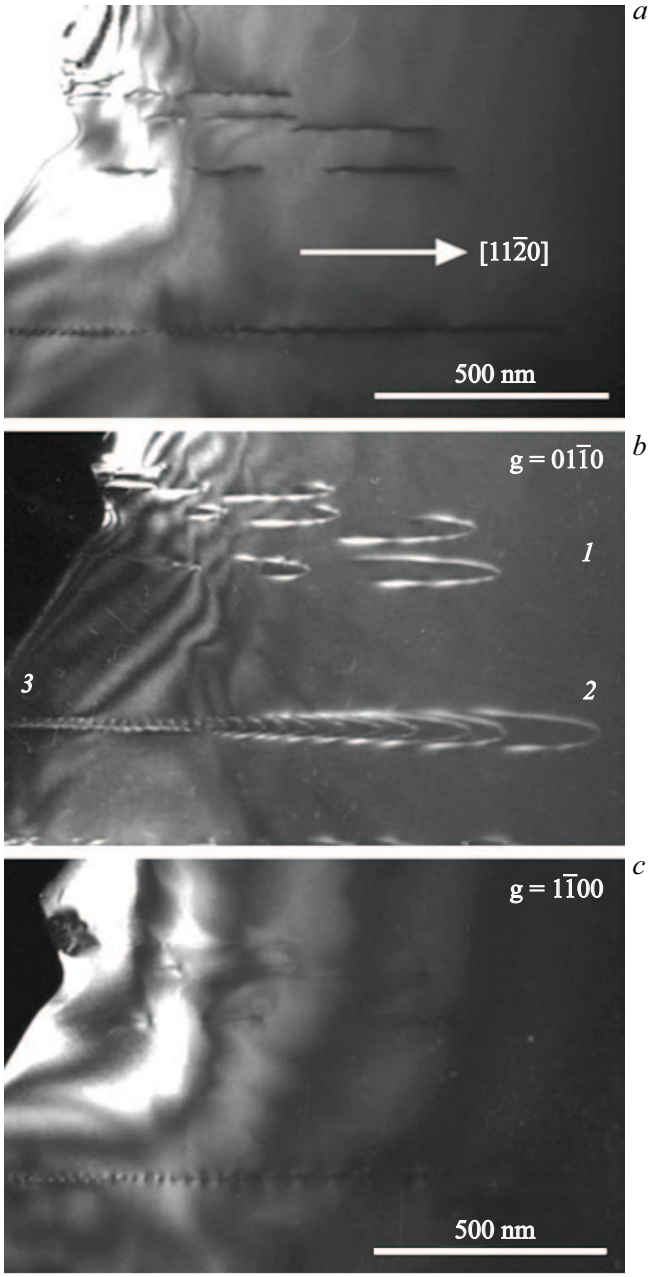

Figure 4. a — propagation of the dislocations from stress concentrators. Reflection 01$\bar{1}$0. Orientation of the sample near the zone axis [0001]; b — semi-loops (*1, 2*) identified as a result of inclination of the sample and the dislocation wall (*3*); c — residual contrast of the same defects in the reflection 1$\bar{1}$00.

The values of D in Fig. 3, *d* and other similar images vary within the interval approximately from 400 to 1000 nm. By estimating the Burgers vector b with a value of about 0.3 nm [16], we obtain that the rotation angle θ is

within the interval approximately from 0.017 to 0.043°. Since the distances between the dislocations vary not only between various images, but within one wall as well, it is possible to satisfy oneself with a simple arithmetic mean of the minimum and maximum values: $\theta \sim 0.03°$.

Another types of defects in the studied samples is microinhomogeneities. Fig. 4 shows dislocations that propagate in the planar sample from the hole edge into the electron-transparent region (Fig. 2). Dislocation sources are arranged at the very edge so that details of their images are indistinguishable. These can be microinclusions or grain boundaries.

The following specific features are obvious in Fig. 4: the lines along $[11\bar{2}0]$ (Fig. 4, *a*); the semi-loops and dislocation assemblies at the levels *1–3*, respectively (Fig. 4, *b*). The lines that look straight with orientation of the sample near the zone axis [0001] (Fig. 4, *a*) are transformed into the semi-loops as a result of heavy inclination of the sample (Fig. 4, *b*). Contrast for the reflections from the three prismatic planes $\{1\bar{1}00\}$ has been analyzed to show that the semi-loops are observed on the dark-field images $01\bar{1}0$ and $10\bar{1}0$ and almost disappear in the reflection $1\bar{1}00$ (Fig. 4, *c*). Therefore, according to the condition $\mathbf{g} \cdot \mathbf{b} = 0$ their Burgers vectors have a component along the direction $[11\bar{2}0]$ and the slip system is prismatic: $\{1\bar{1}00\}\langle 11\bar{2}0\rangle$. Residual contrast in Fig. 4, *c* is related to edge-type head components of the semi-loops.

In order to identify details of the wall of the prismatic dislocations in Fig. 4, *b*, we use a magnified image. A lower left corner in Fig. 5, *a* demonstrates separate dislocations that are included in the wall. They have residual contrast in the reflection $0\bar{1}10$, thereby giving reason to believe that their Burgers vector is parallel to $[\bar{2}110]$. Projections of these dislocations to a basal plane have a different length (Fig. 5, *b*). The increase of the length indicates reduction of an angle between the dislocation line and the basal plane. In a sample location marked by the white arrow, periodicity of dislocation arrangement fails. We believe that this location is a source of the image of the basal plane dislocation. Fig. 5 well demonstrates lines that form a figure as a „tile roof" crowned by a „spire" of two components of the length of $\sim 2\,\mu$m enclosed by an open curve. Images of these lines elongated along $[2\bar{1}\bar{1}0]$ are almost invisible in the reflection $0\bar{1}10$ (Fig. 5, *d*), thereby affirming that the Burgers vectors of the dislocations are in the direction $[\bar{2}110]$ and the configuration in Fig. 5 is formed by screw basal dislocations of the *a*-type.

The screw dislocations of the *a*-type were detected in GaN and thoroughly studied by methods of cathodoluminescence and TEM [17]. In the study [17] the basal dislocations were shaped as gliding semi-loops of screw and edge components that expand in the basal plane. Two factors prevent similarity to a configuration detected in the present study. First of all, the Burgers vectors of the screw basal dislocations have the same signs. Secondly, the curve that enclosed these screw dislocations and whose shape reminds a „head component" is not an edge dislocation. Nevertheless, similarity is that portions of the screw basal dislocations are transformed into the mixed dislocations that easily glide without going out of the basal plane, but changing their initial directions, whereas the dislocation loops in the prismatic planes can only elongate [17].

According to the previously published data, the screw basal dislocations can be converted into the edge threading dislocations that surface or go deep into the sample [17,18]. It is interesting to trace variation of the configuration in Fig. 5 with a distance in the basal plane. Now we turn to Fig. 6, which includes a mutual arrangement of the basal dislocations identified in an adjacent region. In order to understand differences in their visibility, let us remember the following rules. The image of the screw dislocation becomes invisible when $\mathbf{g} \cdot \mathbf{b} = 0$. A purely-edge dislocations disappears in such a reflection when the conditions $\mathbf{g} \cdot \mathbf{b} = 0$ and $\mathbf{g} \cdot \mathbf{n} = 0$ are fulfilled simultaneously. Here, $\mathbf{n}$ is a vector that is perpendicular to a slip plane. The mixed dislocations do not disappear. However, their visibility is the least when the conditions $\mathbf{g} \cdot \mathbf{b} = 0$ and $\mathbf{g} \times \mathbf{b} \cdot \mathbf{u} = 0$ are fully or partially fulfilled, where $\mathbf{u}$ is a vector of a tangent to the dislocation line.

The reflection $2\bar{1}\bar{1}0$ (Fig. 6, *a*) well exhibits all the dislocations with a non-zero value of $\mathbf{b}_a$ along $\langle 11\bar{2}0\rangle$. Let us compare visibility of these dislocations in three reflections from the prismatic planes $\{1\bar{1}00\}$. The lines designated by the letters *A*, *E* and *F* disappear in the reflection $0\bar{1}10$ (Fig. 6, *c*), but are well visible in the reflection $1\bar{1}00$ (Fig. 6, *b*). According to the criterion $\mathbf{g} \cdot \mathbf{b} = 0$, the Burgers vectors of the dislocations *A*, *E* and *F* are oriented along the direction $[\bar{2}110]$. Applying the same criterion to the dislocations *B* and *C*, which extinguish in the reflection $10\bar{1}0$, we conclude that their Burgers vectors are parallel to $[1\bar{2}10]$ (Fig. 6, *d*). Contrast in the portion *G* near intersection of the lines *A* and *B* does not disappear in any of the reflections from the prism

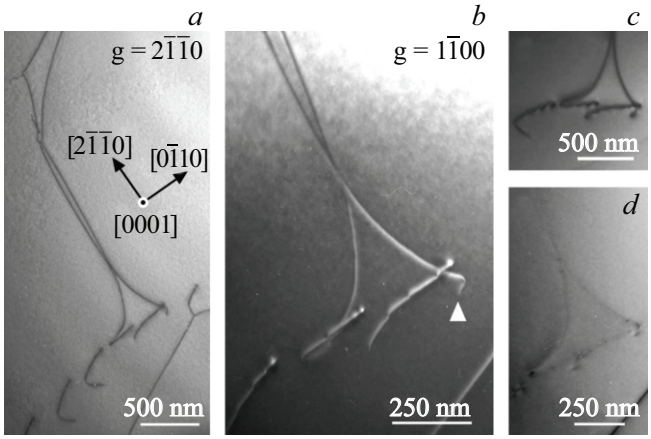

Figure 5. *a* — dislocations of the two slip systems: prismatic (below left) and basal (in the center and up left); *b* — the magnified image; *c, d* — variation of visibility of the basal dislocations in the reflections $10\bar{1}0$ (*c*) and $0\bar{1}10$ (*d*), respectively.

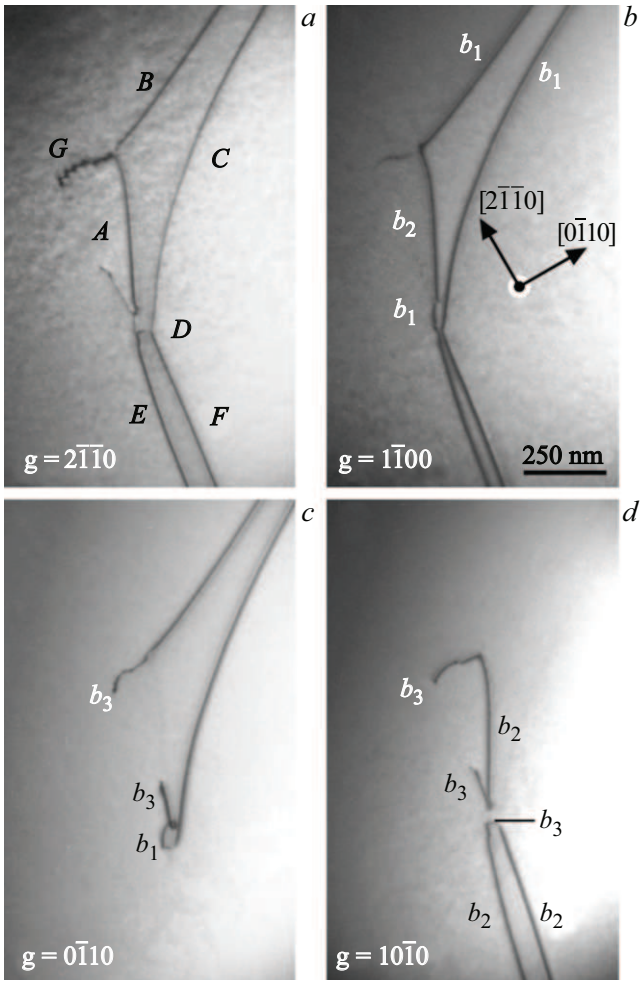

Figure 6. *a* — in the reflection $2\bar{1}\bar{1}0$ the dislocations marked by letters from *A* to *G* have non-zero contrast; *b* — attenuation of visibility of the dislocation *G* in the reflection $1\bar{1}00$; *c, d* — extinction of the dislocations A, E, F and B, C in the reflections $0\bar{1}10$ and $10\bar{1}0$, respectively.

planes. The dislocation *G* has residual contrast in the reflection $1\bar{1}00$, thereby indicating the component $\mathbf{b}_a$ that is parallel to $[\bar{1}\bar{1}20]$. No contrast in the portion *D* when $\mathbf{g} = 10\bar{1}0$ confirms that in this portion the vector $\mathbf{b}$ is oriented along the direction $[1\bar{2}10]$. Near the same location, there is a short branch that is invisible in the reflection $1\bar{1}00$, but has high contrast when $\mathbf{g} = 0\bar{1}10$. It is possible if its vector $\mathbf{b}$ is directed along $[\bar{1}\bar{1}20]$. All the Burgers vectors of the above-described dislocations are designated in Fig. 6 in the following sequence: $\mathbf{b}_1 = \pm(1/3)\ [1\bar{2}10]$; $\mathbf{b}_2 = \pm(1/3)\ [\bar{2}110]$ and $\mathbf{b}_3 = \pm(1/3)\ [\bar{1}\bar{1}20]$.

Conclusion

The AlN single crystal of the thickness of 2.5 mm and the diameter of 64 mm was grown on the SiC substrate by using the improved PVT-technology in presence of the liquid silicon phase on the growing surface. The dislocations in the grown crystal were studied by the TEM method. The above-given analysis demonstrated that the TD density quickly decreases with the distance to the interface due to interaction of the threading dislocations between each other and with groups of other dislocations. In particular, the dislocation walls were straight portions of a limited length along $\langle 10\bar{1}0\rangle$ or $\langle 11\bar{2}0\rangle$. The walls consisted of the dislocations separated by the distances from 400 to 1000 nm and caused inclination of the lattice by the angle $\theta \sim 0.03°$. In addition to the walls, the crystal comprised dislocation semi-loops gliding in the prismatic planes. The most probable cause of generation of these defects were microinhomogeneities.

A quite interesting manifestation of behavior of the inclined threading dislocations glided along the prismatic system was their conversion into the basal dislocations. This variation of the dislocation type and the slip plane was not accompanied by reverse conversion into the threading dislocations. It seems that grazing in the basal plane, which was accompanied by interaction of the dislocations, resulted in reduction of their energy.

Quality of AlN crystallization was improved by presence of the liquid silicon film during growth. It shall be noted that presence of a foreign phase on the surface of the growing crystal required application of the AlN buffer layer over the entire surface of the substrate, since liquid silicon in presence of Al at the growth temperatures about 1950 °C–2000 °C can cause intense etching of the SiC substrate. As a rule, the buffer layer is deposited at the low temperatures $\sim$ 1200 °C by Chemical Vapor Deposition (CVD). We have found conditions of deposition of the AlN buffer layer by the sublimation method, thereby significantly reducing probability of crystal etching during growth and cooling. In-depth study of the slip systems of as-grown dislocations in these crystals contributes to solving some issues (still unclear) of improving the quality of the plates with the industrial size $\geq$ 2 inches.

Acknowledgments

The study used equipment provided by Interdisciplinary Resource Center „Nanotechnologies“ of the St. Petersburg State University as part of the project 125021702335-5.

Funding

The study was carried out under the State assignment of the Ioffe Institute, RAS and the State assignment of Institute for Problems of Mechanical Engineering, RAS.

Conflict of interest

The authors declare that they have no conflict of interest.

References

[1] S.A. Kukushkin, A.V. Osipov. J. Phys. D: Appl. Phys., **47** (31), 313001 (2014). DOI: 10.1088/0022-3727/47/31/313001

[2] S.A. Kukushkin, A.V. Osipov, A. Redkov. In: *Mechanics and Control of Solids and Structures. Advanced Structured Materials*, ed. by V.A. Polyanskiy, A.K. Belyaev (Springer, Cham, 2022), v. 164. DOI: 10.1007/978-3-030-93076-9_18

[3] A.L. Hickman, R. Chaudhuri, S.J. Bader, K. Nomoto, L. Li, J.C.M. Hwang, H.G. Xing, D. Jena. Semicond. Sci. Technol., **36**, 044001 (2021). DOI: 10.1088/1361-6641/abe5fd

[4] R.R. Sumathi. ECS J. Solid State Sc., **10** (3), 035001 (2021). DOI: 10.1149/2162-8777/abe6f5

[5] D. Dojima, K. Ashida, T. Kaneko. J. Cryst. Growth., **483**, 206 (2018). DOI: 10.1016/j.jcrysgro.2017.11.032

[6] C. He, H. Wu, C. Jia, K. Zhang, L. He, Q. Wang, J. Li, N. Liu, S. Zhang, W. Zhao, Z. Chen, B. Shen. Cryst. Growth Des., **21** (6), 3394 (2021). DOI: 10.1021/acs.cgd.1c00170

[7] L. Zhang, H. Qi, H. Cheng, L. Jin, Y. Shi. J. Semicond., **40** (10), 102801 (2019). DOI: 10.1088/1674-4926/40/10/102801

[8] Y. Han, Z. Zhang, W. Hu, W. Wang, J. Guo, L. Guo. Cryst. Growth Des., **24** (4), 1818 (2024). DOI: 10.1021/acs.cgd.3c01483

[9] A.N. Anisimov, I.D. Breev, K.V. Likhachev, O.P. Kazarova, S.S. Nagalyuk, P.G. Baranov, B.Ya. Ber, D.Yu. Kazantcev, M.P. Scheglov, E.N. Mokhov. Semiconductors, **56** (5), 281 (2022). DOI: 10.1134/S1063782622050025

[10] Y. Tokumoto, K. Kutsukake, Y. Ohno, I. Yonenaga. J. Appl. Phys., **112**, 093526 (2012). DOI: 10.1063/1.4764928

[11] J. Chen, K. Chen, X. Su, M. Niu, Q. Wang, K. Xu. Thin Solid Films, **791**, 140240 (2024). DOI: 10.1016/j.tsf.2024.140240

[12] M. Miyanaga, N. Mizuhara, S. Fujiwara, M. Shimazu, H. Nakahata, T. Kawase. J. Cryst. Growth, **300** (1), 45 (2007). DOI: 10.1016/j.jcrysgro.2006.10.233

[13] Y. Yao, Y. Sugawara, Y. Ishikawa, N. Okada, K. Tadatomo. J. Electron. Mater., **49**, 5144 (2020). DOI: 10.1007/s11664-020-08016-x

[14] E.N. Mokhov, A.A. Wolfson, O.P. Kazarova. Phys. Solid State, **61** (12), 2286 (2019). DOI: 10.1134/S1063783419120321

[15] J.P. Hirth, J. Lothe. *Theory of Dislocations* (Wiley, NY., 1982)

[16] Y.N. Picard, M.E. Twigg, J.D. Caldwell, C.R. Eddy Jr., M.A. Mastro, R.T. Holm. Scr. Mater., **61** (8), 773 (2009). DOI: 10.1016/j.scriptamat.2009.06.021

[17] O. Medvedev, O. Vyvenko, E. Ubyivovk, S. Shapenkov, A. Bondarenko, P. Saring, M. Seibt. J. Appl. Phys., **123**, 161427 (2018). DOI: 10.1063/1.5011368

[18] Y. Yao, Y. Sugawara, Y. Ishikawa, N. Okada, K. Tadatomo, Y. Takahashi, K. Hirano. Jpn. J. Appl. Phys., **58**, SCCB29 (2019). DOI: 10.7567/1347-4065/ab0d0a

Translated by M.Shevelev